RSC Advances

ROYAL SOCIETY OF CHEMISTRY

www.rsc.org/advances

This work emphasizes the potential of COOH-functionalized nanodiamond (NDs) particles to improve bio-interactions when embedded into fish gelatin electrospun fibers.

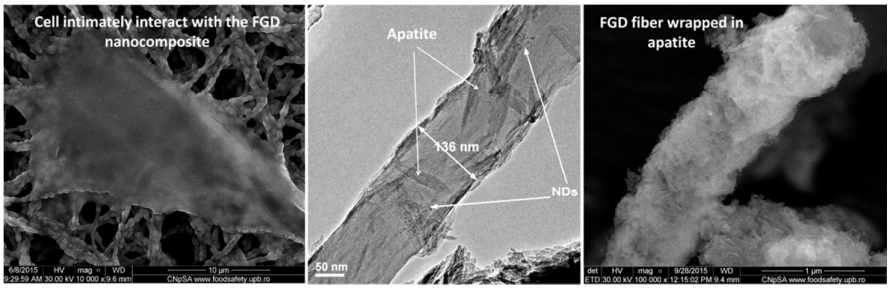

Journal Name

ARTICLE

Electrospun fish gelatin fibrous scaffolds with improved bio-interactions due to carboxylated nanodiamond loading

Received 00th January 20xx,
Accepted 00th January 20xx

DOI: 10.1039/x0xx00000x

www.rsc.org/

A. Serafim [a]†, S.Cecoltan [a]†, A. Lungu [a], E. Vasile [b], H. Iovu [a,c] and I. C. Stancu [a]

Nanotechnology and biomimicry represent appealing but still underexploited techniques to develop innovative scaffolds with ECM-inspired features for tissue engineering. In the present work we have investigated the potential of a combination of two design elements to trigger enhanced bio-interactions with bone regeneration potential: COOH-functionalized nanodiamond particles (COOH-NDPs) have been loaded for the first time into electrospun fish gelatin hydrogel fibers thus generating nanocomposite fibrous scaffolds with interconnected porosity. When compared to control fish gelatin fibers, no significant modification of the mineralization capacity in acellular simulated body fluid has been put into evidence by micro-structural and spectroscopic investigations, for fibers with COOH-NDPs content ranging from 0.25% to 1%. It is important to mention that, following Ca/P alternate incubation, nano-apatite crystals were preferentially developed and firmly adhered on the fibers regions in the proximity of COOH-NDPs, as proven by transmission electron microscopy (TEM). Significant mineralization occurred in culture media in the presence of MG63 osteoblasts-like cells and seem to be directly stimulated by the presence of the nanoparticles. Altogether, these findings emphasize the ability of NDPs to enhance, when immobilized in gelatin fibers and exposed to specific media, the formation of apatite. It was also noticed that the number of adherent MG63 cells, their morphology and spreading were improved by increasing the amount of NDPs in the fibers (fluorescence and scanning electron microscopy). This work successfully proves the potential of such nanocomposite fibers to find applications in bone regeneration.

Introduction

While tissue engineering allows the design of biological substitutes to repair or replace damaged organs or tissues, nanotechnology related research provides the means for mimicking the morphologic features of the extracellular matrix (ECM). The use of nanostructures in combination with polymer matrices has become an appealing approach to improve the performances of a scaffold. The high surface to volume ratios of nanoparticles is responsible for a number of improved behaviors such as increased capacity to interact with the host matrix, enhanced ability to adsorb cell adhesion proteins or other biologically-relevant species, as well as higher mechanical properties. Nanocomposites are multiphase materials containing at least one type of nanostructures. One of the most intensively studied natural nanocomposites is the ECM of hard tissues. Its extraordinary mechanical strength may be attributed to the composition and intimate interaction between its main constituents: nano-apatite as inorganic phase and collagen fibrils within the hydrogel matrix. The modern design of biomaterials for scaffold-assisted bone regeneration often starts with an approach inspired by this nanocomposite. The development of nanostructured composite scaffolds based on biomimetic nanoparticles and hydrogels appears as a promising route for mimicking the natural environment of cells. Whereas nano-apatite/hydrogel composites are widely explored in this aim [1], the development of nanocomposites based on nanodiamond particles (NDPs) and hydrogels recently gained increased attention. NDPs are biomimetic nanostructures demonstrating, in addition to excellent mechanical properties and chemical inertness, higher biocompatibility when compared to other carbon-based species such as carbon black, single- and multi-walled carbon nanotubes (SWNTs, MWNTs) [2,3]. Only limited research describe NDPs-reinforced apatite coatings and films developed for medical metal materials [4,5] or composites with biomineralization ability, based on NDPs and biodegradable polymers [6,7]. Despite the potential of these materials, applications are still lacking and NDPs-hydrogel composites are still underexplored. In the present study we have investigated the potential of gelatin loaded with carboxylated NDPs to promote bio-interactions necessary for bone regeneration. It is generally accepted that natural biomineralization is controlled by the macromolecular matrix of hard tissues. In this respect,

[a] Advanced Polymer Materials Group, Faculty of Applied Chemistry and Material Science, University Politehnica of Bucharest, 1-7 Gh Polizu Street, Sector 1, 011061 Bucharest, Romania.E-mail: izabela.cristina.stancu@gmail.com.
[b] University POLITEHNICA of Bucharest, Faculty of Applied Chemistry and Material Science, Department of Science and Engineering of Oxide Materials and Nanomaterials, No. 1-7 Gh Polizu Street, 011061 Bucharest, Romania
[c] Academy of Romanian Scientists, 54 Splaiul Independentei, Bucharest 050094, Romania

† These authors contributed equally to this work.
See DOI: 10.1039/x0xx00000x

we have used gelatin as biopolymer component due to appealing properties such as collagenous origin, cell-interactive, easy to crosslink leading to hydrogels, biodegradable, widely investigated to produce scaffolds for various biomedical applications [8–16]. In addition to the ECM-inspired composition, keeping in mind the fibrillary structure of the hard tissues ECM, ultrafine fibrous scaffolds based on gelatin loaded with dispersed NDPs were produced through electrospinning. This processing technique has recently gained interest in the preparation of scaffolds for tissue regeneration since it leads to fibrous mats with open porosity, large surface area to volume ratio and flexibility [14,17–19]. No attempts to fabricate gelatin fibers containing dispersed nanodiamonds have been reported yet, to the best of our knowledge. Gelatin-graphene oxide nanocomposites have been electrospun for the first time in 2014 [14].

Due to the risk of transmitting diseases such as bovine spongiform encephalopathy as well as to some socio-cultural constrains associated to the widely investigated mammalian gelatin, fish gelatin (FG) was used in this work [20,21]. Cold water FG has lower gelation temperature allowing enhanced processing at room temperature [22] that can be accordingly associated with enhanced electrospinning from more concentrated aqueous solutions with respect to mammalian gelatins. In this context, in this work electrospun nanodiamond-FG fibers were obtained and characterized. Moreover, the bone-binding ability of artificial scaffolds is enhanced by the ability to induce bone-like apatite formation after implantation in a living body or by the presence of apatite coatings. Anionic species such as –COOH groups are extensively studied for their potential to promote biomimetic mineralization [23–25]. In this respect we decided to carboxylate NDPs before fibers electrospinning. The investigation of the response of the nanocomposite fibers to *in vitro* mineralization tests and to apatite coating procedures becomes mandatory when aiming scaffolds for bone regeneration. Furthermore, it is of outermost interest to establish the bio-interactions of these new nanocomposites with MG63 cells and to verify the effect of the carboxylated NDPs on cell attachment and growth.

Experimental

Materials

Gelatin from cold water fish skin (FG) and glutaraldehyde (GA) 25% aqueous solution were purchased from Sigma. Diamond nanopowder (NDPs), <10 nm particle size (TEM), ≥95% trace metals basis was received from Aldrich. H_2SO_4 (97%) (Fluka) and HNO_3 (70%) (Aldrich) were used to oxidize NDPs. The simulated body fluid (SBF) was prepared using sodium chloride (Fluka), sodium hydrogen carbonate (Fluka), potassium chloride (Riedel de Haen), dipotassium hydrogen phosphate trihydrate (Fluka), magnesium chloride hexahydrate (Fluka), calcium chloride (Sigma-Aldrich) and sodium sulfate (Sigma-Aldrich). Hydrochloric acid was acquired from Sigma-Aldrich and used as 1M aqueous solution. Tris (tris-hydroxymethylaminomethane) was also purchased from Sigma-Aldrich and used as such. The procedure was previously described in [24]. Calcium chloride and sodium phosphate dibasic (Sigma) were used as mineralization precursors for alternate incubation. Double distilled water (ddH_2O) obtained with a GFL 2102 apparatus was used throughout all experiments.

Preparation of electrospun (COOH-NDPs)-loaded FG fibrous scaffolds

Carboxylated diamond nanoparticles (COOH-NDPs) were obtained through the surface carboxylation of NDPs using an oxidizing procedure adapted from [26]. Briefly, acid treatment (97% H_2SO_4 and 70% HNO_3 at a v/v ratio of 3:1) was applied to NDPs in a sonication bath, at a concentration of 0.25% w/v. The suspension was poured into ddH_2O at 80°C and stirred for 10 h. The treated NDPs were subsequently washed with large amounts of ddH_2O under continuous stirring, at room temperature, and then recovered following successive centrifugations and dried at 80°C for 24 h. Fibrous scaffolds were obtained through the electrospinning of FG aqueous solutions (50% w/w) containing various ratios of COOH-NDPs (COOH-NDPs/FG, w/w): 0%, 0.25%, 0.5% and 1%. The nanoparticles were dispersed at room temperature for 16 h using magnetic stirring, followed by sonication in an ultrasound bath (Elma S 30H, Elmasonic), for an additional 8 h. A modular electrospinning set-up developed in our laboratory was used (KDS model 100 injection pump, Glassman 75 W high voltage source, rotating collector). The used electrospinning parameters were: G30 needle, applied voltage of 28 kV, working distance between the electrodes of 110 mm, flow rate of 0.3 ml h^{-1}, collector's rotation speed of 400 rpm, injection volume 0.8 ml. The fabrication of the fibrous mats was performed at room temperature, without any prior heating of the suspensions. Crosslinking was performed on fibers detached from the collector, rolled on polyethylene supports and subsequently placed in vapor saturated atmosphere of glutaraldehyde (GA) for seven days, at room temperature. For simplicity, the crosslinked fibers will be further denoted as FGD-0, FGD-0.25, FGD-0.5 and FGD-1, respectively.

Characterization of the scaffolds

Attenuated total reflectance Fourier transform infrared (ATR-FTIR) spectrometry was performed on a Jasco 4200 spectrometer equipped with a Specac Golden Gate ATR device, using a resolution of 4 cm^{-1}, in the 4.000–600 cm^{-1} wavenumber region and 100 scans. A K-ALPHA (Thermo Scientific) X-ray photoelectron spectrometer (XPS) was employed to study the carboxylation of NDPs, operated as previously described [24]. Fluorescence microscopy was performed on a Nikon TE2000U microscope equipped with a 5MP cooled CCD camera and 4x long working distance objective. The morpho-structural features of gold-sputtered fibrous scaffolds were examined through scanning electron microscopy (SEM) using a QUANTA INSPECT F SEM device equipped with a field emission gun (FEG) with 1.2 nm resolution and with an X-ray energy dispersive spectrometer

(EDX). Transmission electron microscopy (TEM) was also used in order to depict the scaffolds in various stages of the study. The micrographs were registered using a TECNAI F30 G2 S-TWIN microscope operated at 300 kV with EDX and EELS facilities. The images acquired for the crosslinked scaffolds provided information regarding fibers diameter and NDPs size and distribution. TEM micrographs were also registered both after one and three cycles of Ca/P incubation. In this respect, a small piece of fibrous scaffold was deposited on a TEM copper grid and covered with a thin amorphous carbon film with holes. Single fibers were observed at the edge of the scaffolds. High resolution TEM (HRTEM) micrographs were also registered using the same equipment. Micrographs were taken from randomly chosen areas on the grid to ensure representative imaging. Evaluation of the mechanical properties of the hydrated FGD samples was performed using a CT3 texture analyzer with a cell load of 4500 grams (Brookfield CT3), in compression mode. Three cylindrical samples (60 mm diameter and 77 mm height) were tested using a TA44 compression probe (d=4 mm) to a deformation of 50% at a testing speed of 0.1 mm/s. A stress-deformation curve was plotted and the elasticity modulus was calculated for each composition, at 5% strain.

Evaluation of *in vitro* mineralization in acellular conditions

The fibrous scaffolds were immersed in 1 x simulated body fluid (SBF) as described in [27], at physiological pH and temperature. Incubation was performed for 3 and 14 days. SBF was prepared as previously reported [24] and renewed every 48 hours. After incubation, the samples were gently rinsed three times with ddH_2O to remove residual salts physically attached to the mats and dried at 37°C. SEM and TEM micrographs were recorded in order to evaluate the *in vitro* mineralization potential of the synthesized composite fibrous scaffolds.

Coating with apatite through Ca/P alternate incubation

After the crosslinking treatment and purification with ddH_2O, the scaffolds were alternatively immersed in $CaCl_2$/Na_2HPO_4 solutions to induce biomimetic apatite formation, according to the protocol described by Taguchi et al [28]. The scaffolds response to the alternating mineralization baths was investigated after one and three cycles of incubation, respectively. One cycle of incubation refers to incubation in 0.5 M $CaCl_2$ solution for 30 minutes, followed by incubation in an equivalent volume of 0.3 M Na_2HPO_4 solution for the same period of time. As in previous tests, after each incubation period, the samples were gently rinsed with ddH_2O in order to remove residual salts physically attached to the fibers.

Cell culture

Preparation of fibrous scaffolds for cell seeding. In order to obtain suitable samples for cell culture tests, the above mentioned protocol was modified as follows: (1) the precursors were sterilized by passing through 0.45 µm PVDF syringe driven filters (Milipore) prior to electrospinning; (2) the GA solution used as crosslinker was also filtered using the same procedure; (3) when the crosslinking was complete, the samples were washed three times with Tris-HCl 50mM pH 7.4 solution, followed by three times washing with PBS pH 7.4 (Sigma) and finally with Dulbecco's Modified Eagle Medium (DMEM)(Sigma-Aldrich) supplemented with 10% fetal bovine serum (FBS) (Biochrome) and 100 U/mL penicillin-streptomycin (Merck). All maneuvers were performed under the biological hood so that to avoid any possible contamination.

Cell seeding. MG63 human osteosarcoma cell line were cultured for 7 days in DMEM supplemented with 10% FBS and 2 mM L-glutamine penicillin-streptomycin at 37°C in a humidified atmosphere with 5% CO_2. The non-adherent cells were removed after one day; the medium was changed every 48 hours throughout the experiment. The cells were detached by trypsin/ EDTA (Merck Millipore) at 80% confluence in the view of further use.

Cell adhesion on fibrous scaffolds. The scaffolds, prepared as previously described, were seeded with MG63 cells at a density of 10^4 cells/well for 18h for adherence tests and $5x10^3$ cells/well for 7 days for proliferation tests, respectively. Subsequently, all samples were incubated in complete culture medium at 37°C in a humidified atmosphere with 5% CO_2 in a flat bottom 96-well tissue culture plates (TCP). Cell-adherent TCP was used as control sample. To investigate cells' morphology and adherence on the prepared scaffolds, the samples were suitably prepared for SEM analyses. In this respect at the end of each time point the medium was discarded and samples were rinsed with PBS, pH 7.4, fixed with PBS solution containing 4% (w/v) paraformaldehyde for 1 h at room temperature and rinsed twice with PBS. Subsequently, the samples were dehydrated with a gradient of ethanol (Sigma, >99%). The micrographs were recorded using a QUANTA INSPECT F50 SEM device equipped with a field emission gun (FEG) with 1.2 nm resolution.

Fluorescence microscopy (FM) was an alternative technique used to investigate cells adherence on substrates with various NDPs loading ratios. The analyses were performed using a Nikon TE2000U microscope equipped with a 5MP cooled CCD camera with long working distance objectives of 4x and 20x, respectively. For each field, separate grey scale images (16bit TIFF) were taken using GFPHQ filter blocks (SG – λEx 445-485, λEm 500-540, PI – lEx 510–560 nm, lEm 590–600 nm). The scaffolds were rinsed with PBS, pH 7.4, fixed with paraformaldehyde PBS solution (4% w/v) for 1 h, rinsed twice with PBS and permeabilized with 0.1% Triton X-100 (Merck). In order to better visualize the cells, the seeded scaffolds were stained with Sybr green while the cytoskeleton was stained using Phaloidine FITC-red (Lifetechnologies). FM images corresponding to samples at 24 hours post-seeding were processed using ImageJ software. In this respect, five randomly selected areas were used for nuclei cells count. The average count was graphically represented.

To investigate scaffolds' influence on cell morphology, seven random images were selected for each composition and subsequently analyzed using CellProfiler software. The perimeter was quantified and the form factor was computed following a protocol adapted from [29]. Form factor values (ratio

of area to perimeter) are used to quantify cellular extension [30]. The value of this parameter is considered 1 for a perfectly round cell and 0 when the cell has an infinite number of cellular extensions.

Statistical analysis

The statistical data were obtained using Student t-test. Differences were considered significant for $p < 0.05$.

Results and discussion

In this work we report, for the first time, the development of a simple method to generate nanodiamond-reinforced gelatin electrospun fibers using nanoparticles - FG aqueous suspensions, in non-toxic conditions. The method allows the effortless fabrication of nanocomposite fibers using water as solvent with an increased gelatin content (50% w/w), without additional heating (above room temperature). Such synthesis conditions become very important when compared to previous works reporting the preparation of gelatin-based electrospun scaffolds using bovine gelatin dissolved in organic solvents [9,31] or needing heating at 30°C or 50°C [8], with concentration of the protein in the precursor solution of maximum 30-40% [8,32]. We also stipulated the method to crosslink the fibers. In addition to the fabrication of the nanocomposite electrospun fibers and to such technical optimization, this study is important since it investigated the potential of carboxylated nanodiamonds to promote bio-interactions when dispersed, at low concentration, into fish gelatin ultrathin fibers.

NDPs carboxylation

Since anionic groups are widely investigated for their potential to stimulate biomineralization of polymer scaffolds [24,33], we initially oxidized the nanoparticles before electrospinning. The success of the surface carboxylation was studied through ATR-FTIR and XPS analyses. In addition to typical FTIR stretching vibrations at 3409 cm^{-1}, 1720 cm^{-1} and 1641 cm^{-1}, assigned to strong O-H and C=O stretching, a new strong peak appears at 1097 cm^{-1} and it is attributed to C-O stretching vibration from -COOH groups [34] (Fig. 1a).

XPS spectra provided additional evidence on the presence of -COOH groups after the acid treatment. The C(1s) spectrum confirmed, after deconvolution, the presence of sp^2 carbon at binding energies of 284.8eV and sp^3 carbon at 285.5eV (Fig 1b,c). Oxygen-bonded carbon species were also investigated and the presence of –COOH groups was confirmed, on the oxidized particles, through a new peak at a binding energy of 288.1 eV, in agreement with reported data [35]. The increase of the O/C ratio after the oxidation (from 10.19% to 13.74%), as calculated from the ratio of the peak areas O(1s) to C(1s) may be also considered an additional proof of the carboxylation. Altogether, these data confirm the successful carboxylation of NDPs.

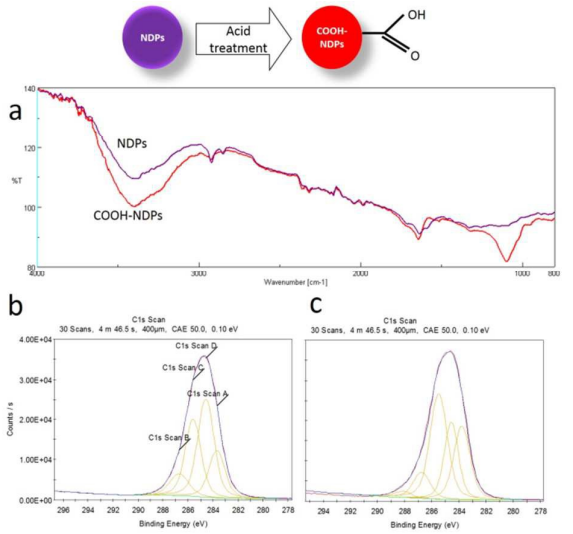

Fig. 1: a) ATR-FTIR spectrum of nanostructures, before (NDPs) and after the oxidation (COOH-NDPs). A new strong peak appears at 1097 cm^{-1} and it is attributed to C-O stretching vibration from -COOH groups. C(1s) XPS spectra of b) NDPs and c) COOH-NDPs. A new peak appears at 288.1 eV, assigned to COOH

Morphology of the crosslinked COOH-NDPs-loaded FG fibrous scaffolds

No significant differences were noticed between the synthesized nanocomposite materials: homogeneous fibers, continuous, with smooth surface, without bead defects along their axes, with average diameters of approximately 230nm, entangled into mats with interconnected porosity. The reported electrospinning conditions were optimized after a delicate procedure to control the fibers properties. It is generally accepted that due to the high water-affinity of gelatins, even a drop of water can destroy the submicronic fibrillary structures. Therefore, crosslinking was performed and the efficiency of the treatment was verified by immersion in ddH_2O at physiologic temperature for 24 hours. All the scaffolds kept their initial appearance: fibrous with uniform non-woven morphology as demonstrated in Fig.2 (a-d). No significant differences were noticed between the nanocomposites (Fig.2b-d) and the control hydrogel (Fig.2a). TEM analyses provided information on the distribution of the nanoparticles into the fibers. Very important, the nanostructures (measured diameters between 2.5 ÷ 7 nm) are immobilized into the polypeptide, however, COOH-NDPs are not homogeneously dispersed into the hydrogel, a tendency to form chain-like aggregates along the axes of the fibers was noticed, as visible in Fig.2e and Fig. 2f.

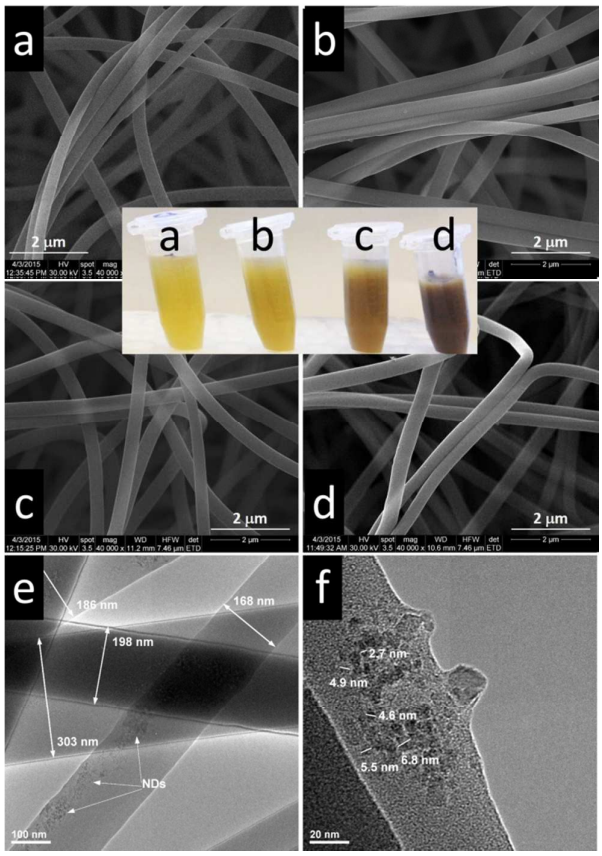

Fig. 2: SEM images of crosslinked electrospun fibers (scale bar 2µm): a)FGD-0, b) FGD-0.25, c) FGD-0.5, d) FGD-1 (digital photo of precursors containing dispersed COOH-NDPs). TEM micrographs of FGD-1 scaffolds: e) fibers with chain-like aggregates of nanoparticles; f) COOH-NDPs in a fiber.

Compression testing

Compression testing was performed in order to assess the mechanical properties of the materials and the effect of different COOH-NDPs content. Elasticity modulus augmented with increasing the amount of nanostructures into the hydrogels. The increase of the elasticity modulus when compared to FGD-0 is almost negligible for FGD-0.25 (2%, from 1.38 ± 0.3 MPa to 1.41 ± 0.02 MPa). FGD-0.5 is characterized by a 1.53 ± 0.01 MPa elasticity modulus, corresponding to an increase of 11% with respect to the control hydrogel FGD-O. The highest COOH-NDPs loading is associated with an increase with 25% of the elasticity modulus (1.73 ± 0.05 MPa). These data indicate that the nanoparticles have a reinforcing role decreasing the elasticity of the resulting nanocomposite material. Such effect on the mechanical behavior was expected since on one hand NDPs are among the hardest materials and, on the other hand, they restrict the movement of the macromolecular chains. Our results are in agreement with other works reporting the enhancement of the elasticity modulus following incorporation of nanodiamond into polymers such as poly(vinyl alcohol) [36] and poly (L-lactide-co-e-caprolactone) (poly(LLA-co-CL)) scaffold [37].

The change in mechanical properties due to addition of nanodiamonds, combined with the surface chemistry and the high surface-to-volume ratio of these nanostructures are expected to enhance the biointeractions with the cellular medium stimulating the activity of MG63 cells on the tested scaffolds.

***In vitro* mineralization in acellular conditions**

Mineral formation in a given matrix is crucial for bone regeneration since it would generate a composite with intimate interactions between its phases, similar to bone ECM. In order to evaluate the stability and the *in vitro* mineralization capacity of the nanocomposite fibrous scaffolds, samples of each composition were incubated in physiologically-relevant acellular simulated media for 3 and 14 days, respectively. Incubation in SBF is reported in many studies as an adequate acellular method to predict mineralization behavior of a material *in vitro* [24,38,39]. The stability of the scaffolds and the presence of new *in vitro*-formed mineral after incubation in SBF for 3 and 14 days, respectively, were micrographically explored by SEM. The integrity of the fibers was not affected during the test, as proved by the general fibrous appearance in SEM micrographs (Fig. 3). The presence of the nanoparticles at loadings lower than 1% was not associated with mineral formation after 3 or 14 days. After 3 days, on the surface of the FGD-1 fibers, low mineralization occurrence was noticed, as isolated small calcified nodules (Fig. 3b). Increasing the incubation time leads to needles and plate-like mineral structures grown from and onto the fibers (Fig. 3c). This new phase, not continuously coating the fibers, is morphologically similar to biological apatite, in agreement with previously published data [24]. We have shown in a different work that the formation and distribution of apatite nuclei (followed by growth into larger elongated structures, called in their early stages fibrils) appeared to be initiated by agglomerated -COOH groups from carboxylated gold nanoparticles coating a polymer substrate [24]. In a similar way, the mineral formed on FGD-1 may be assigned to the presence of COOH- groups on the surface of NDPs. When compared to the mineralization on polymer surfaces coated with COOH-functionalized gold nanoparticles [24], the effect noticed here is less efficient, probably due to the very low amount of nanoparticles in the fibers and also to the fact that the nanostructures are distributed into the fibers.

Coating with apatite through alternate Ca/P incubation

Coating with apatite is an appealing solution to increase the integration of implants and the interaction with bone cells, due to the high biological affinity of this mineral to natural bone [24]. The development of apatite-coated electrospun fibrous scaffolds prepared from bovine gelatin B has been recently achieved [9]. The authors reported that on the first day (corresponding to one cycle of incubation), mineral particles were formed and discontinuously deposited on the surface of the fibers.

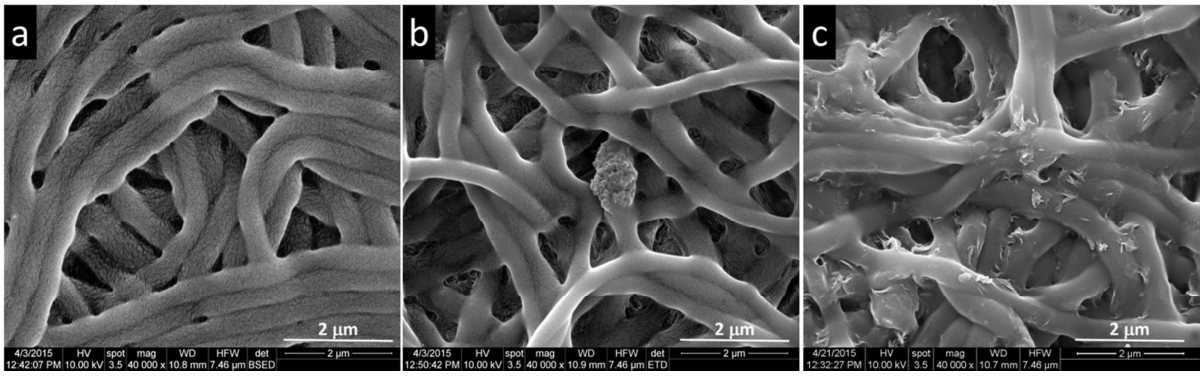

Fig. 3: SEM micrographs of the fibrous scaffolds after 3 days in SBF a) FGD-0 fibers with no mineralization, b) FGD-1 with isolated calcified nodulus; c) SEM image of thin mineral elongated elementary structures grown on the surface of FGD-1 after 14 days in SBF.

Similarly, we performed an alternate incubation of FGD-1 nanocomposites in Ca/P baths to verify the efficiency of the biomimetic apatite formation and the effect of COOH-NDPs, if any. Representative morpho-structural features characteristic to the mineralization of FGD-1 in comparison to FGD-0 are shown in Fig. 4. Similarly to the electrospun bovine gelatin fibers from a different work [9], FGD-0 was covered by mineral nanostructures forming a discontinuous layer after one cycle of incubation and completely wrapping the fibers after 3 cycles. SEM investigations identified areas from where the thick mineral was detached (Fig.4a) probably due to brittleness as well as to week interactions between the deposited inorganic phase and the macromolecular fibers. After only one cycle of incubation the FGD-1 fibers were discontinuously covered with a thin mineral layer with morphological features characteristic to apatite: agglomerated polycrystalline structures formed by elongated elementary particles (Fig. 4b) as we previously reported [24]. The nanocomposite fibers have the appearance of coral branches, non-coated areas are still visible (Fig. 4b). As the mineralization time was increased to 3 cycles of alternate Ca/P incubation, a thick and dense layer of Ca-P mineral wrapped the FGD-1 fibers as visible in the SEM micrograph from Fig. 4c.

TEM analyses provided complementary morphological and microstructural data on the mineral formation. The inorganic phase deposited on FGD-0 consists in elongated needles and plate-like particles that seem to detach easily from the polymer fibers (Fig. 4d). Needle-like mineral was identified by TEM on FGD-1 fibers, strongly adhering to the nanocomposite mesh (Fig. 4e). The TEM micrographs revealed that crystallites were preferably formed in the proximity of agglomerated COOH-NDPs, suggesting the potential of these nanostructures to act as mineralization promoters, under specific conditions, or to strongly interact with the mineral phase (Fig 4e). As expected, after 3 cycles a dense layer of inorganic crystallites were identified on FGD-1 (Fig. 4f).

The micrographs from Fig. 4g-i show morphological evidences of the presence of nanostructured calcium-phosphate phase. Selected area electron diffraction (SAED) and FFT analysis identified crystallographic planes typical to apatite: (211), (301), (213), (321), (511), also confirmed by the HRTEM images (Fig. 4i). In addition, EDX microanalysis indicated that the mineral phase formed after the incubation has a ratio Ca/P of 1.67 ± 0.002 on FGD-1, similar to the stoichiometry of apatite (Ca/P of 1.67) while the value for FGD-0 is 1.34 ± 0.005. These results suggest that the use of COOH-NDPs enhance the affinity of FGD fibers for calcium simultaneously stimulating a higher compatibility between the macromolecular fibers and the newly formed mineral phase.

Cell adhesion on fibrous scaffolds

The nanocomposites fibrous scaffolds were explored in regard to the effect of the COOH-NDPs on number and morphology of adhered cells. Initially, the results were assessed by fluorescence microscopy. MG63 osteoblasts adhered on the NDPs-containing scaffolds (FGD-0.25 ÷ FGD-1), as well as on the FGD-0 control fibers and the plastic dish (Fig. 5).

Increasing the content of nanostructuring agent in the fibers from 0 to 1% (Fig.5a-d) was directly associated with higher adhesion. The highest number of cells was detected on FGD-1 (Fig.5d,i). Similar results were reported with respect to the development of MG63 on gelatin-based fibers and on gelatin-apatite electrospun fibers [40]. However, this study is the first report on the improvement of MG63 cell adhesion by increasing nanodiamond content in FG-COOH-NDPs electrospun nanocomposites. At 7 days, no significant difference was visible by fluorescence microscopy. All scaffolds are completely covered by a confluent layer of cells (Fig. 5e-h).

Adhesion and spreading of anchorage-dependent cells such as osteoblasts are essential for the estimation cell-scaffold biointeractions. A stretched morphology is characteristic for a strong anchorage of osteoblasts, while rounder cell geometries are typical for less adhesive substrates [29].

Journal Name

ARTICLE

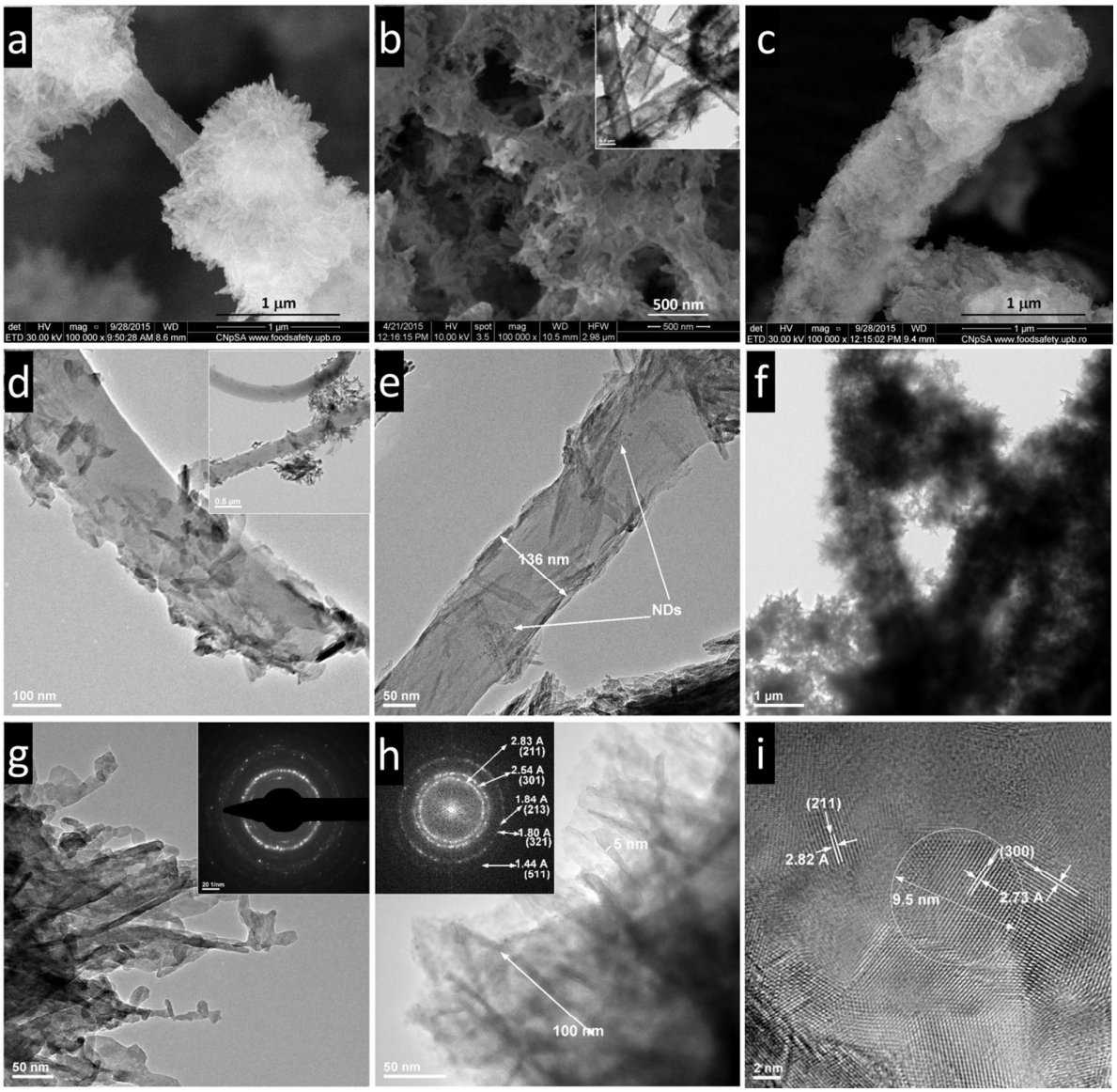

Fig.4: Fibers after Ca/P incubation. a) SEM micrograph of FGD-0 fiber covered with a thick and brittle mineral layer after 3 cycles (the mineral detached easily from the fiber); b) SEM image of FGD-1 fibers coated by elongated thin inorganic particles, sparsely aggregated on the surface of the fibers, after 1 cycle (inset – representative TEM image); c) SEM image of FGD-1 fiber wrapped in a dense uniform mineral layer formed after 3 cycles; d) TEM image of a FGD-0 fiber with mineral thin plate-like nodules discontinuously deposited onto the polymer surface after 3 cycles (inset – fibers with lowly adhered mineral elongated plate-like nodules and clusters); e) TEM micrograph showing mineral elongated crystallites formed and strongly adhered to the surface of a FGD-1 fiber in the close proximity of agglomerated COOH-NDPs, after 1 cycle; f) TEM image of calcified FGD-1 after 3 cycles; g) elongated and plate-like nanostructures formed on FGD-0 after 3 cycles with SAED image; h) elongated nanostructures formed on FGD-1 after 3 cycles with SAED image displaying typical crystallographic planes characteristic to apatite: (211), (301), (213), (321) and (511); i) HRTEM image of apatite nanocrystals with characteristic planes (211), (300) developed after 3 cycles on FGD-1 (a nanocrystal with diameter of 9.5 nm is shown in the white circle)

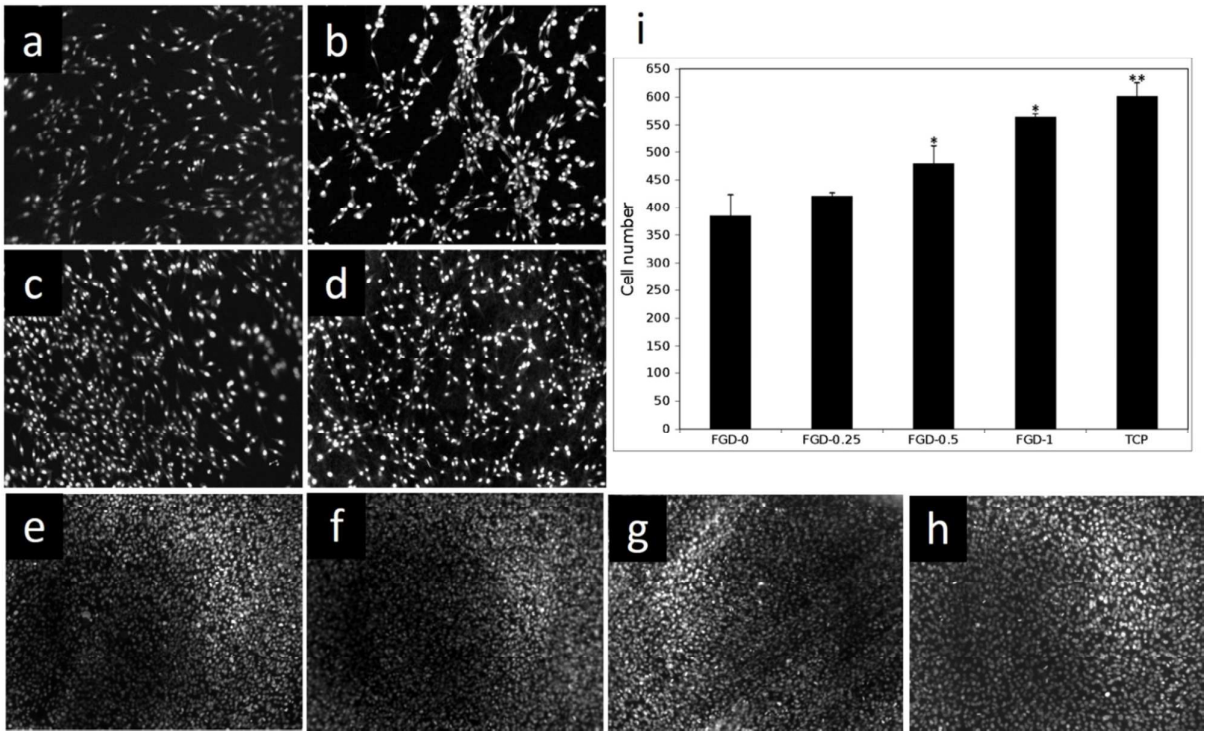

Fig. 5: MG63 seeded on nanocomposite fibrous scaffolds at 24 hours: a – FGD-0, b – FGD-0.25, c – FGD-0.5, d– FGD-1, and at 7 days: e – FGD-0, f – FGD-0.25, g – FGD-0.5, h– FGD-1; i – Cell number – composition dependence at 24 hours; nuclei stained with Sybr Green (*p < 0.05, **p < 0.01).

To investigate the effect of NDPs loading on the adhesive properties of the FGD nanocomposite fibers, the morphological features of MG63 cells were evaluated at 24 hours post-seeding and a cytometric study was performed. Thin cells with flat spindle shaped morphology, having membranes in intimate contact with the nanostructured fibers, were observed on the scaffolds containing increased NDPs amount (Fig.6).

Image analysis performed using CellProfiler software showed that the highest perimeter and the lowest form factor values were determined for FGD-1 (Fig.6e). More specifically, even though the lowest NDPs amount used influenced the morphology of cells, significant differences were noticed at loading exceeding 0.5%.

In addition to FM and cytometric analysis, SEM assessment of the overall cellular morphology and individual cytoskeleton in terms of shape and area confirmed the previously described cell behavior. These results broaden the understanding of the effect of nanodiamonds embedded into FG hydrogel fibers on the behavior of cells. They represent an early indication on the ability of such nanocomposite scaffolds to guide osteoblasts attachment.

Accordingly, it can be concluded that the nanocomposite fibers containing 0.5% and 1% NDPs, respectively, promoted enhanced spreading and stronger adhesion of MG63 cells with respect to the fibers with the lowest nanoparticles content (0.25%) or NDPs-free fibers. These findings are promising for the use of FGD nanocomposite fibrous scaffolds in bone regeneration.

However, the potential adverse effects of using nanodiamonds in such biomedical substrates cannot be excluded. Considering that the matrix of the FGD nanocomposite fibers is biodegradable, the nanodiamonds would be released and accumulate in the body due to their non-biodegradability.

The potential cytotoxicity of the nanodiamond particles remains a controversial and still underexplored issue to be further elucidated, despite of the recognized advantages including higher biocompatibility when compared to other carbon nanospecies such as MWCNs and SWCNs [41]. Some reports exist on the unfavorable behavior of NDPs [42,43]. Other studies report that the use of NDPs in various scaffolds, even at relatively higher loading when compared to our FGD scaffolds did not elicit damaging effects. For example 23% NDPs loaded in PLGA fibers did not evoke considerable inflammatory response on MG63 and RAW 264.7 cells [44], and PLLA-based composites with up to 10% ND-ODA are non-cytotoxic for murine 7F2 osteoblasts cells [45]. Moreover, microinjected NDPs in worm gonads were found to not affect the longevity and reproductive potential of C. elegans [46].

In this context, advanced studies on the biological effects associated with the presence of NDPs in FGD scaffolds including biodegradation testing will be performed in the future.

Journal Name

ARTICLE

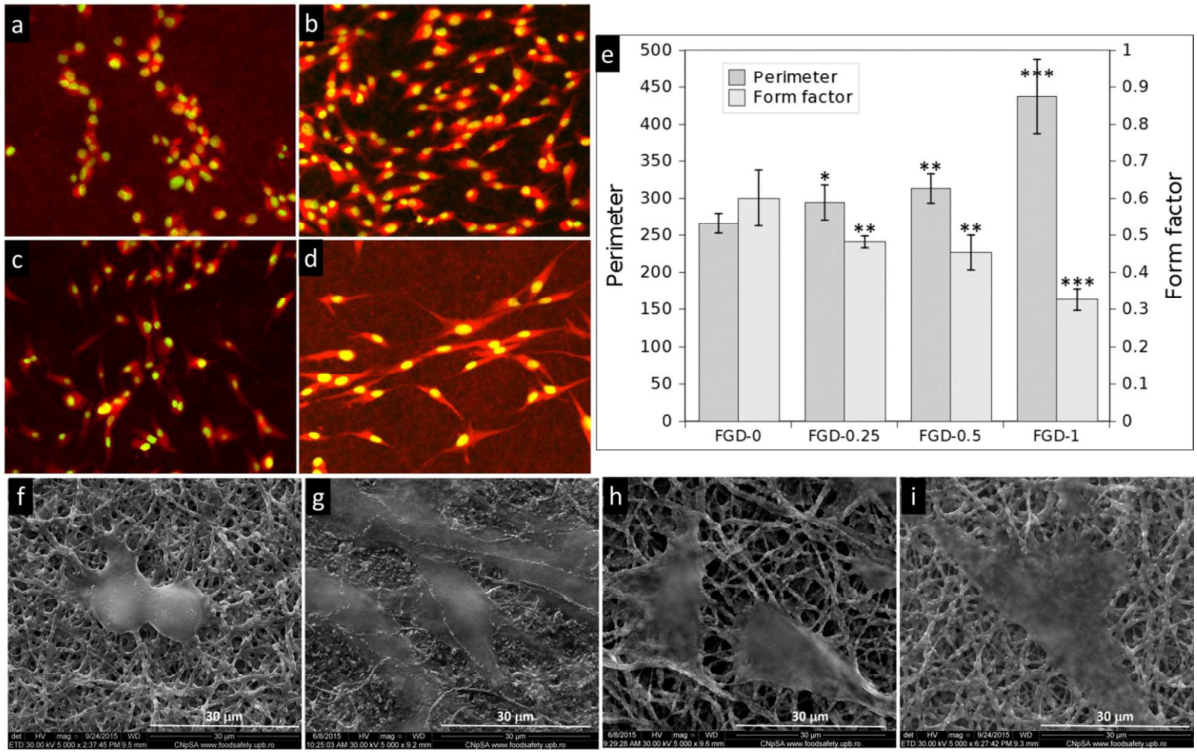

Fig.6. MG63 cells adhered at 24 h post seeding - nuclei were stained with Sybr Green and the cytoskeleton was stained with Phalloidin red for the determination of form factor: a) FGD-0; b) FGD-0.25; c) FGD-0.5; d) FGD-1; e) influence of the composition on the perimeter and form factor (*p < 0.05, **p < 0.01, ***p < 0.001); SEM micrographs of MG63 cells at 24 h post seeding on: f) FGD-0; g) FGD-0.25; h) FGD-0.5; i) FGD-1; mineral clusters are formed on the fibrous scaffolds.

Mineralization in cellular conditions

Formation of mineral is reported in cultures of osteoblastic cells [47,48]. Therefore besides from revealing the cellular behavior, the MG63 cell culture tests were used in this study to investigate additional bio-interactions with the FGD matrices. It was noticed by SEM that an accelerated mineral nucleation and growth occurred after only 24 hours on all cell seeded scaffolds (Fig.6f-i and Fig. 7a-d), with respect to incubation in SBF. Calcium phosphates generated by cellular uptake of Ca/P ions initiate the development of mineral. Differences in the distribution and geometry of the formed inorganic deposits on the nanocomposite fibers with respect to the control hydrogel were noticed. Calcified mineral clusters were developed discontinuously on the fibers, similarly to the coating generated by alternate incubation in Ca/P baths. While clusters consisting in few agglomerated needles and thin plates are developed on the control FGD-0 hydrogel fibers (Fig. 7a), mineralized areas richer in nano-sized nuclei were formed on the nanostructured materials containing increasing NDPs amounts (Fig. 7b-d). Higher NDPs loading in the nanocomposites was also associated with denser mineral deposits along the fibers, FGD-1 being almost completely wrapped in inorganic islands (Fig. 7d). The hydrogel permeability allows ions to penetrate the nanocomposite fibers, subsequently promoting mineral nucleation in the proximity of –COOH groups. It can be speculated that, in addition to –COOH groups from gelatin, the increased amount of exposed carboxylates from the oxidized NDPs with hard and inert cores and high surface-to-volume ratio lead to denser nucleation areas, reducing, in the next steps, the size of apatite crystallites.

Longer incubation time additionally stimulated the development of the calcified aggregates. SEM showed that the mineral phase progressively developed and expanded along the FGD fibers. Moreover, spheroidal satellites emerging from the initial mineral coating were epitaxially developed after 7 days, as visible in Fig. 7e-l).

In Fig 7e it can be observed that the FGD-0 fibers are not totally coated with mineral at 7 days in cell culture conditions. A second generation of spheroidal calcified nodules are formed on the initial mineral areas, while non-calcified polymer areas are still observed. The loading with NDPs seem again to stimulate a stronger calcification when compared to FGD-0. Accordingly, FGD-0.25 (Fig.7f) and FGD-0.5 (Fig.7g) present a stronger diffusion of the calcified areas along the fibers but they remain discontinuously covered. Increasing the incorporation of nanodiamond to 1% was associated with the highest calcification when compared to the other samples. At the end of the 7th day, FGD-1 fibers are completely wrapped in a continuous mineral layer on which a second generation of mineral started to form, appearing as numerous calcospherites (Fig. 7h). The mineral phase formed on all the materials is nanostructured (Fig. 7i-l). EDX spectra revealed Ca/P ratios with value of 1.23 ± 0.02 on FGD-o and 1.66 ± 0.03 on FGD-1. This suggests again a higher concentration of calcium on the samples containing nanodiamond, and a mineral with a stoichiometry close to that of apatite, similarly to the results observed after the alternate Ca/P incubation. Moreover, it was observed that the cell membrane is intimately interacting with the calcified inorganic layer formed on the nanocomposite fibers loaded with NDPs, as showed in Fig. 6g-i. The cells adhered on the FGD-0 scaffolds had a rounder shape (Fig. 6f). We will further investigate this calcification in the future, to better describe the interaction of cells with such nanocomposites. We believe that the presence of the oxidized nanodiamond in the hydrogel fibers enhance the affinity for calcium ions stimulating the mineral formation and further promoting higher cell-interactivity of the scaffold.

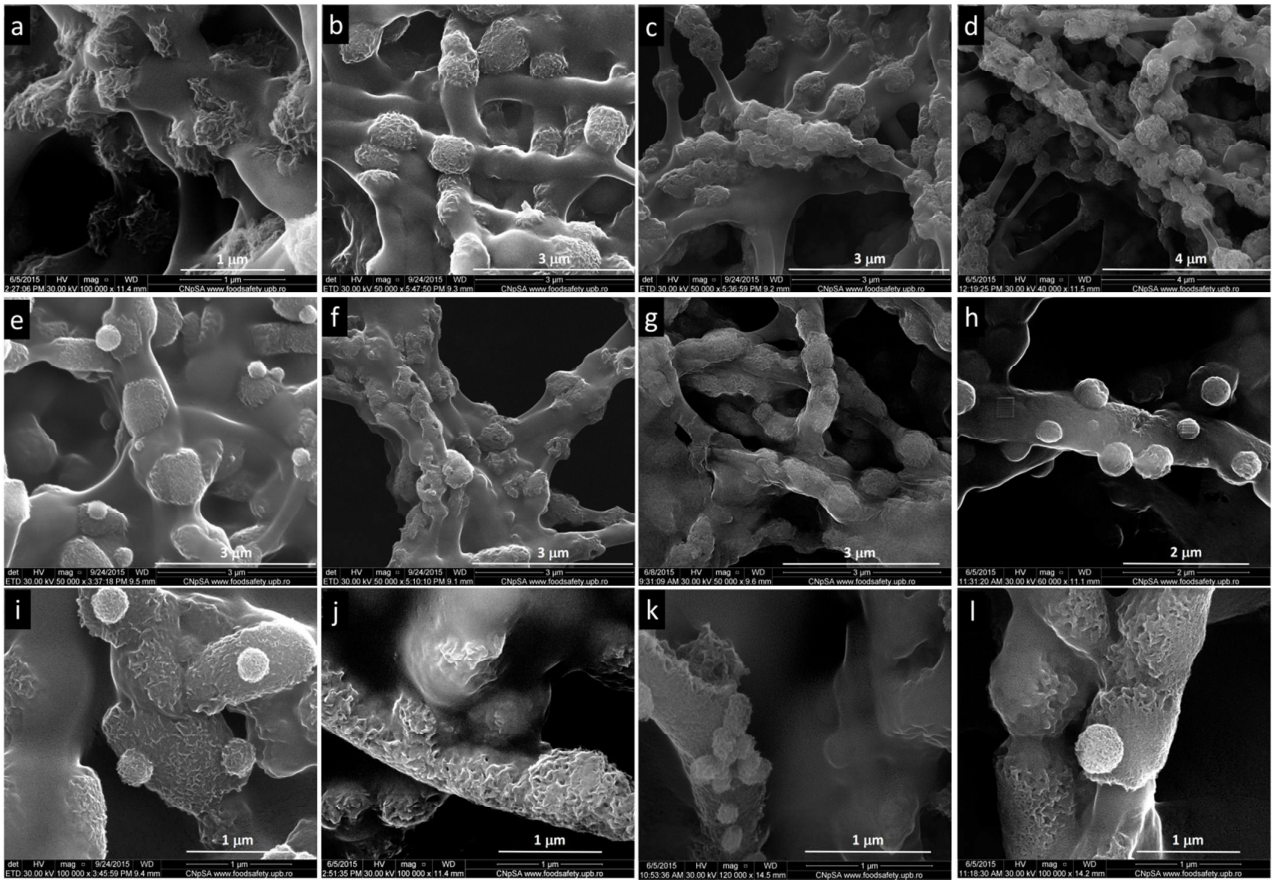

Fig.7. SEM micrographs of nanostructured calcified nodules deposited in cell culture medium after 24 h (a-d) and after 7 days (e-l) on: a, e, i – FGD-0; b,f,j – FGD-0.25; c,g,k – FGD-0.5; d,h,l – FGD-1. Nanostructured mineral phase is visible in i-l.

Conclusions

This study presents, for the first time, a simple synthesis method for the synthesis of nanostructured fibrous scaffolds based on FG and COOH-NDPs, using a 50% w/w FG aqueous solution, electrospun at room temperature. Even the synthesis itself opens new research directions due to an innovative combination of (1) fish gelatin - NDPs nanocomposites (not yet investigated to the best of our knowledge), (2) effortless electrospinning procedure using non-toxic solvents, at room temperature (the studies available so far on electrospun gelatins report the use of organic solvents [9,31] and/ or elevated temperatures [8,32]). Moreover, this work emphasizes the potential of COOH-NDPs to improve bio-interactions when embedded into the studied biopolymer, even at low dispersion ratios.

In summary, the *in vitro* studies reported here unequivocally suggested that COOH-NDPs - gelatin nanocomposite electrospun fibers have the potential to promote enhanced mineralization when compared to pristine gelatin fibers. In addition to the mineralization induced by -COOH groups of the hydrogel[9], the nanoparticles influenced the development of mineral phase, possibly through increased affinity for calcium ions from the simulated fluids, leading to mineral nucleation and growth. Such behavior can be easily explained through the high surface-to-volume ratio and increased amount of exposed -COOH groups from the NDPs. Overall, the nanostructuring with carboxylated NDPs stimulates biomineralization and enhances cell adhesion. However, future studies are required to better describe and control such behavior for tissue engineering applications.

Acknowledgements

The work has been funded by the Sectorial Operational Programme Human Resources Development 2007-2013 of the Ministry of European Funds through the Financial Agreement POSDRU/159/1.5/S/132397. Also the authors would like to acknowledge the financial support from the project 183/2012, Bioactive Injectable Macroporous Biomaterials for Bone Regeneration. The SEM analyses on cell seeded scaffolds were possible due to EU-funding grant POSCCE-A2-O2.2.1-2013-1/Axa prioritara 2, Project No. 638/12.03.2014, cod SMIS-CSNR 48652. Dr. Celina Damian is gratefully acknowledged for the XPS analysis.

Notes and references

1 N. Sasaki, H. Umeda, S. Okada, R. Kojima and A. Fukuda, *Biomaterials*, 1989, **10**, 129–132.
2 Y. Zhu, J. Li, W. Li, Y. Zhang, X. Yang, N. Chen, Y. Sun, Y. Zhao, C. Fan and Q. Huang, *Theranostics*, 2012, **2**, 302–312.
3 A. M. Schrand, L. Dai, J. J. Schlager, S. M. Hussain and E. Osawa, *Diam. Relat. Mater.*, 2007, **16**, 2118–2123.
4 M. S. Amin, L. K. Randeniya, a. Bendavid, P. J. Martin and E. W. Preston, *Diam. Relat. Mater.*, 2009, **18**, 1139–1144.
5 E. Pecheva, L. Pramatarova, T. Hikov, D. Fingarova, Y. Tanaka, H. Sakamoto, H. Doi, Y. Tsutsumi and T. Hanawa, *Surf. Interface Anal.*, 2010, **42**, 475–480.
6 Q. Zhang, V. N. Mochalin, I. Neitzel, K. Hazeli, J. Niu, A. Kontsos, J. G. Zhou, P. I. Lelkes and Y. Gogotsi, *Biomaterials*, 2012, **33**, 5067–75.
7 L. Ivanova, C. Popov, I. Kolev, B. Shivachev, J. Karadjov, M. Tarassov, W. Kulisch, J. P. Reithmaier and M. D. Apostolova, *Diam. Relat. Mater.*, 2011, **20**, 165–169.
8 S. Zhang, Y. Huang, X. Yang, F. Mei, Q. Ma, G. Chen, S. Ryu and X. Deng, *J. Biomed. Mater. Res. Part A*, 2009, **90A**, 671–679.
9 J. Zhao, Y. Zhao, Q. Guan, G. Tang, Y. Zhao, X. Yuan and K. Yao, *J. Appl. Polym. Sci.*, 2011, **119**, 786–793.
10 I.-C. Stancu, A. Lungu, D. M. Dragusin, E. Vasile, C. Damian and H. Iovu, *Soft Mater.*, 2013, **11**, 384–393.
11 I.-C. Stancu, *React. Funct. Polym.*, 2010, **70**, 314–324.
12 D.-M. Dragusin, S. Van Vlierberghe, P. Dubruel, M. Dierick, L. Van Hoorebeke, H. A. Declercq, M. M. Cornelissen and I.-C. Stancu, *Soft Matter*, 2012, **8**, 9589.
13 A. Serafim, D. G. Petre, L. Moraru, H. E. Cioflan, E. Vasile, B. Mastalier, M. Petrutescu and I. C. Stancu, *Key Eng. Mater.*, 2015, **638**, 38–46.
14 S. Panzavolta, B. Bracci, C. Gualandi, M. L. Focarete, E. Treossi, K. Kouroupis-Agalou, K. Rubini, F. Bosia, L. Brely, N. M. Pugno, V. Palermo and A. Bigi, *Carbon N. Y.*, 2014, **78**, 566–577.
15 A. Serafim, C. Tucureanu, D.-G. Petre, D.-M. Dragusin, A. Salageanu, S. Van Vlierberghe, P. Dubruel and I.-C. Stancu, *New J. Chem.*, 2014, **38**, 3112.
16 A. Serafim, D. M. Draguşin, L. M. Butac, D. S. Vasilescu, P. Dubruel and I. C. Stancu, *UPB Sci. Bull. Ser. B Chem. Mater. Sci.*, 2013, **75**, 3–14.
17 J. Zhao, S. Jiang, R. Zheng, X. Zhao, X. Chen, C. Fan and W. Cui, *RSC Adv.*, 2014, **4**, 51696–51702.
18 A. K. Jaiswal, S. S. Kadam, V. P. Soni and J. R. Bellare, *Appl. Surf. Sci.*, 2013, **268**, 477–488.
19 N. Bhardwaj and S. C. Kundu, *Biotechnol. Adv.*, 2010, **28**, 325–47.
20 A. A. Karim and R. Bhat, *Food Hydrocoll.*, 2009, **23**, 563–576.
21 R. Jeya Shakila, E. Jeevithan, A. Varatharajakumar, G. Jeyasekaran and D. Sukumar, *Food Chem.*, 2012, **135**, 2260–2267.
22 B. S. Chiou, R. J. Avena-Bustillos, J. Shey, E. Yee, P. J. Bechtel, S. H. Imam, G. M. Glenn and W. J. Orts, *Polymer (Guildf).*, 2006, **47**, 6379–6386.
23 E. Murugan and S. Arumugam, *RSC Adv.*, 2014, **4**, 35428–35441.
24 E. Vasile, A. Serafim, D.-M. Dragusin, C. Petrea, H. Iovu and I.-C. Stancu, *J. Nanoparticle Res.*, 2012, **14**, 918.
25 E. Vasile, A. Serafim, D. Petre, D. Giol, P. Dubruel, H. Iovu and I. C. Stancu, *ScientificWorldJournal.*, 2014, **2014**, 103462.
26 A.-Y. Jee and M. Lee, *Curr. Appl. Phys.*, 2009, **9**, e144–e147.
27 J. A. Sowjanya, J. Singh, T. Mohita, S. Sarvanan, A. Moorthi, N. Srinivasan and N. Selvamurugan, *Colloids Surf. B. Biointerfaces*, 2013, **109**, 294–300.
28 T. Taguchi, Y. Muraoka, H. Matsuyama, A. Kishida and M. Akashi, *Biomaterials*, 2000, **22**, 53–58.
29 A. E. Carpenter, T. R. Jones, M. R. Lamprecht, C. Clarke, I. H. Kang, O. Friman, D. a Guertin, J. H. Chang, R. a Lindquist, J. Moffat, P. Golland and D. M. Sabatini, *Genome Biol.*, 2006, **7**, R100.
30 C. Wang, R. R. Varshney and D.-A. Wang, *Adv. Drug Deliv. Rev.*, 2010, **62**, 699–710.
31 H. Aoki, H. Miyoshi and Y. Yamagata, *Polym J*, 2015, **47**, 267–277.

32 S. R. Gomes, G. Rodrigues, G. G. Martins, C. M. R. Henriques and J. C. Silva, *Mater. Sci. Eng. C. Mater. Biol. Appl.*, 2013, **33**, 1219–27.
33 R. Filmon, F. Grizon, M. F. Baslé and D. Chappard, *Biomaterials*, 2002, **23**, 3053–3059.
34 S. A. Rakha, N. Ali, Y. A. Haleem, F. Alam, A. A. Khurram and A. Munir, *J. Mater. Sci. Technol.*, 2014, **30**, 753–758.
35 Y. Xue, Z. Wang, J. Wang, C. Hu, F. Xie, D. Chen and Z. He, *ISRN Spectrosc.*, 2012, **2012**, 1–6.
36 S. Morimune, M. Kotera, T. Nishino, K. Goto and K. Hata, *Macromolecules*, 2011, **44**, 4415–4421.
37 Y. Sun, A. Finne-Wistrand, T. Waag, Z. Xing, M. Yassin, A. Yamamoto, K. Mustafa, D. Steinmüller-Nethl, A. Krueger and A.-C. Albertsson, *Macromol. Mater. Eng.*, 2015, **300**, 436–447.
38 M. Thomas, A. Arora and D. S. Katti, *Mater. Sci. Eng. C. Mater. Biol. Appl.*, 2014, **45**, 320–32.
39 I. . Stancu, R. Filmon, C. Cincu, B. Marculescu, C. Zaharia, Y. Tourmen, M. . Baslé and D. Chappard, *Biomaterials*, 2004, **25**, 205–213.
40 H. W. Kim, J. H. Song and H. E. Kim, *Adv. Funct. Mater.*, 2005, **15**, 1988–1994.
41 A. M. Schrand, J. Johnson, L. Dai, S. M. Hussain, J. J. Schlager, L. Zhu, Y. Hong and E. Osawa, 2009.
42 Y. Xing, W. Xiong, L. Zhu, E. Osawa, S. Hussin and L. Dai, *ACS Nano*, 2011, **5**, 2376–2384.
43 A. V Karpukhin, N. V Avkhacheva, R. Y. Yakovlev, I. I. Kulakova, V. A. Yashin, G. V Lisichkin and V. G. Safronova, *Cell Biol. Int.*, 2011, **35**, 727–733.
44 M. Parizek, T. E. L. Douglas, K. Novotna, A. Kromka, M. A. Brady, A. Renzing, E. Voss, M. Jarosova, L. Palatinus, P. Tesarek, P. Ryparova, V. Lisa, A. M. dos Santos, P. H. Warnke and L. Bacakova, *Int. J. Nanomedicine*, 2012, **7**, 1931–1951.
45 Q. Zhang, V. N. Mochalin, I. Neitzel, I. Y. Knoke, J. Han, C. A. Klug, J. G. Zhou, P. I. Lelkes and Y. Gogotsi, *Biomaterials*, 2011, **32**, 87–94.
46 N. Mohan, C.-S. Chen, H.-H. Hsieh, Y.-C. Wu and H.-C. Chang, *Nano Lett.*, 2010, **10**, 3692–3699.
47 H. A. Declercq, R. M. H. Verbeeck, L. I. F. J. M. De Ridder, E. H. Schacht and M. J. Cornelissen, *Biomaterials*, 2005, **26**, 4964–4974.
48 K. Yamazaki, S. Ichimura, T.D. Allen, T. Nakagawa, *JBMM*, 1989, **7**, 6-17.